RMetS

Royal Meteorological Society

Effect of the Gulf Stream on winter extratropical cyclone outbreaks

Jill Nelson and Ruoying He*

Department of Marine, Earth, and Atmospheric Sciences, North Carolina State University, Raleigh, NC, USA

*Correspondence to:
R. He, Department of Marine,
Earth, and Atmospheric Sciences,
North Carolina State University,
Raleigh, NC, USA.
E-mail: rhe@ncsu.edu*

Abstract

A high-resolution, regional coupled air–sea model is used to investigate the effect of the Gulf Stream (GS) on surface wind convergence during winter extratropical cyclone (ETC) outbreaks in January 2005 off the east coast United States. Validations against marine buoy-observed surface wind, sea level pressure (SLP), air temperature and sea surface temperature (SST) show decent model skill. Model analyses indicate that the surface wind convergence and the Laplacian of SLP and SST are proportionate on the synoptic time scale. Strong upward vertical motions and ocean heat loss over the GS support rapid ETC intensification. Copyright © 2012 Royal Meteorological Society

Keywords: air–sea interactions; coupled model; Gulf Stream; winter extratropical cyclones

1. Introduction

The Gulf Stream (GS) is a warm ($>24\,°C$) western boundary current that flows northeastward along the eastern North America continental margin. In winter strong heat flux and surface winds associated with the sharp GS horizontal ocean temperature gradients cause energetic air–sea interactions, rapidly destabilizing the marine atmospheric boundary layer (MABL) and influencing the development of synoptic storms (Song *et al.*, 2006; Small *et al.*, 2008). During January in particular, frequent (2–4 per month) and intense (average maximum winds of 23 m s^{-1}) winter extratropical cyclones (ETC) form within or just north of the GS near Cape Hatteras and track along the northeast coast of the United States (Colucci, 1976; Zishka and Smith, 1980; Hirsch *et al.*, 2001). While it is known that such rapidly intensifying east coast ETCs develop offshore along the leading edge of a cold, dry air mass, near the strongest sea surface temperature (SST) gradients, and in regions of surface convergence and upper level divergence (Sanders and Gyakum, 1980), quantitative understanding of air–sea interactions during intense winter ETCs has been hindered due to the lack of high-resolution observations that can resolve both temporal and spatial variability of ETCs. In this regard, the Genesis of Atlantic Lows Experiment (GALE) of winter 1986 was the largest field program ever conducted (Dirks *et al.*, 1988). Concurrent atmospheric and oceanic datasets collected during GALE were used in several observational (Bane and Osgood, 1989; Doyle and Warner, 1990; Holt and Raman, 1990) and modeling (Huang and Raman, 1988; Raman and Reddy, 1996; Xue *et al.*, 2000) studies to understand air–sea interaction processes important for rapid winter cyclone development.

Coupled air–sea modeling has been long recognized as an important and effective means for studying the mechanisms controlling rapid ETC intensification in data sparse regions. Xue *et al.* (2000) coupled a two-dimensional atmospheric model with a two-dimensional ocean model and found large surface heat fluxes and locally enhanced winds off the southeastern United States in a cold air outbreak observed during GALE. That work shows surface winds increase by as much as 75% over the GS which has a significant impact on the upper ocean temperature and velocity fields. Li *et al.* (2002) used a three-dimensional coupled model to investigate spatial heat flux patterns during the passage of a winter storm and found that the central pressure dropped sharply as the cyclone encountered the large heat flux gradients at the shoreward side of the GS. Recent studies by Minobe *et al.* (2008, 2010) aimed to elucidate the GS's influence on the surface wind field. Utilizing QuikSCAT satellite wind data and ECMWF model output, these studies show the mean surface wind convergence on both seasonal and annual time scales exhibits coherent structures along the GS, a result that is further corroborated by Joyce *et al.* (2009). The temporal mean of surface wind convergence is stronger in winter than summer. The atmospheric response to GS-induced surface convergence is confined to the MABL in winter but reaches to the tropopause in summer.

To complement these earlier wind convergence analyses on seasonal and annual time scales, we apply here a newly developed high-resolution, regional coupled air–sea model to simulate winter ETC outbreaks in January 2005 and assess wind field adjustments over the GS on the synoptic time scale. We describe the configuration of the coupled model and model validations in the Model and Data section. The section on

Model Analysis presents detailed wind convergence analysis followed by the Summary and Conclusions section.

2. Model and data

2.1. Coupled air−sea model

We used the Coupled Ocean-Atmosphere-Wave-Sediment-Transport (COAWST) model, which is a newly developed system designed for studying physical interaction processes that effect environmental changes in coastal oceans (Warner *et al.*, 2010). The COAWST configuration is comprised of the Weather Research and Forecasting (WRF) atmospheric model (Skamarock *et al.*, 2008) and the Regional Ocean Modeling System (ROMS) ocean circulation model (Shchepetkin and McWilliams, 2005). Data exchange between concurrent WRF and ROMS simulations is handled by the Model Coupling Toolkit (Larson *et al.*, 2005). Time steps for WRF and ROMS are 60 and 300 s, respectively. During the simulation, wind stress and net heat flux generated by WRF and SST by ROMS are exchanged on each coupling time interval, which is 600 s.

The coupled simulation runs from 13 to 31 January 2005, during which time four east coast ETCs and one 'bomb' [defined by Sanders and Gyakum (1980) as a surface cyclone with a decrease in sea level pressure (SLP) of at least 1 mb h^{-1} for 24 h] ETC occurred. The model domain encompasses central and eastern North America, the Gulf of Mexico, and the northwestern Atlantic Ocean (Figure 1). Given that the strongest ETCs formed just offshore of the east coast of the United States, the model analysis is focused over the western Atlantic Ocean centered at Cape Hatteras, NC. The WRF grid has 15 km horizontal resolution and 48 vertical terrain following levels from sea level to 100 mb. The ROMS grid is configured with 5 km horizontal resolution and 18 vertical terrain following levels with better resolution in the upper ocean. The Spherical Coordinate Remapping and Interpolation Package (Jones, 1998) program included in COAWST is used to create interpolation weights between the different model grids. Once the weights are computed, wind stress and net heat flux from WRF are interpolated to the ROMS grid and SST from ROMS is interpolated to the WRF model grid. Initial conditions and boundary information for WRF are provided by the 32 km, 3 h NCEP North American Regional Reanalysis (http://www.esrl.noaa.gov/psd/data/gridded/data.narr.html) data, whereas initial and boundary conditions for ROMS are obtained from the 10 km, daily HYCOM/NCODA global ocean model simulation (http://www.hycom.org/dataserver).

Examinations of marine meteorological buoy time series (not shown) indicate that during the first half of January 2005 (1−12 January), calm southerly winds
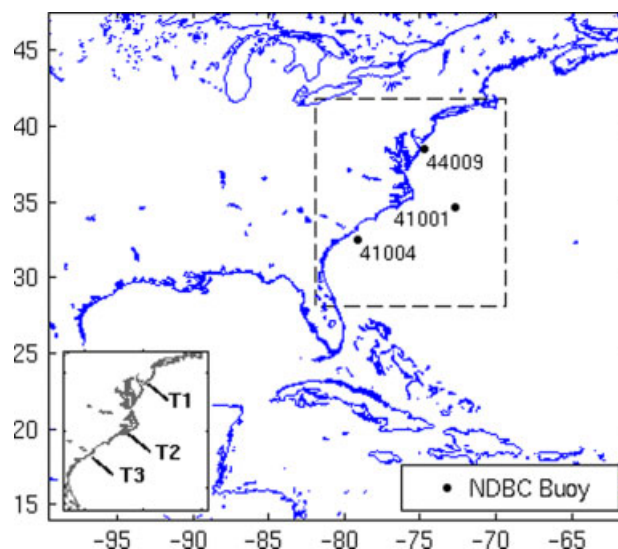

Figure 1. The model domain for the coupled WRF and ROMS simulation (outer box). The dashed box highlights our east coast study region. Also shown are locations of three NDBC marine buoys and three cross-shelf transects (bottom left inset panel) along which vertical profiles of MABL wind fields are diagnosed.

prevailed with mild air temperatures that were about the same as the ocean temperature. In contrast, the second half of month (13−31 January) was characterized by cold air outbreaks following each ETC with sharp drops (up to 20 °C) in surface air temperature, a steady decrease in SST up to 5 °C, and significant sensible and latent heat fluxes out of the ocean (in excess of 600 W m^{-2} total flux in the storm track). Our study is intended to highlight the stormy second half of the month in order to understand the dynamics involved in the strong air−sea interactions in the study area.

2.2. Model validation

In situ observations of near-surface winds, SLP, air temperature, and SST measured by the National Data Buoy Center (NDBC) buoys 44 009, 41 001, and 41 004 were utilized to validate the coupled model simulation. These *in situ* data were sub-sampled every 3 h to be concurrent with the coupled model output over the time period 13−31 January 2005. These buoys measure three distinct ocean regions (Figure 1): the cold mid-shelf waters north of Cape Hatteras (buoy 44 009), the seaward side of the GS offshore of Cape Hatteras (buoy 41 001), and the warm mid-shelf waters south of Cape Hatteras (buoy 41 004). Each model-data wind time series comparison is quantified by a vector correlation coefficient (r), the vector orientation difference (Θ) between observed and model-simulated winds (measured in degrees counterclockwise from true north), and a vector regression coefficient (measuring to what degree the model over- or underestimates the wind speed magnitude). The remaining comparisons are quantified by their correlation coefficient (r) and root mean square error (RMS error).

The coupled model simulation reproduces observations well. The correlation coefficients (Table I)

Table I. Statistic measures of time series comparisons between observed and simulated wind vectors, SLP, air temperature (T), and SST at marine buoys 44009, 41001, and 41004.

Buoy	Wind comparisons r/Θ/regression	SLP comparisons	T comparisons r/RMS error	SST comparisons
44009	0.92/−2.5/1.06	0.99/1.45	0.96/1.96	0.97/0.59
41001	0.84/−3.9/0.91	0.98/1.70	0.97/2.69	0.96/0.47
41004	0.93/−9.0/0.99	0.98/1.62	0.96/2.65	0.02/1.75

between observed and modeled winds range from 0.84 to 0.93. Modeled wind orientations agree to between −2.5° and −9.0° with near-perfect amplitudes (regression coefficients being 0.91–1.06 where anything over 1.0 indicates that the model overestimated magnitudes). The correlations for SLP are 0.98 or higher with mean offsets of less than 1.70 hPa. The air temperature comparisons are also good at all stations, with correlations 0.96 or better and mean offsets less than 2.7 °C. We note that the buoy air temperature sensors have a cold bias due to ocean surface evaporation resulted from storm-induced wave breaking (J. Bane, pers. comm.), which explains at least in part the ∼2.5 °C offset between buoy-observed and model-simulated air temperature. SST comparisons are reasonable as well except at buoy 41004. At that location, small lateral movements of the GS are not captured by the 5 km resolution ocean model, resulting in a low correlation at this station. Nevertheless, SST time series are highly correlated (>0.96) with less

than 0.6 °C bias at the other two stations (44009 and 41001). On the basis of the favorable comparisons at these and other (not shown) sites, we conclude that our coupled model produced realistic simulations of oceanic and atmospheric conditions during the ETC outbreaks in January 2005, lending confidence that dynamical analysis described below is couched in a realistic air–sea environment.

3. Model analysis

With temporally and spatially continuous model fields, we begin by analyzing the synoptic mean surface wind convergence during the ETC outbreak from 13 to 31 January 2005 (Figure 2(a)). Surface wind convergence is calculated as $-(u_x + v_y)$, where u and v are the mean 10 m eastward and northward wind velocity components, respectively. A broad band of convergence is seen off the southeastern US coast
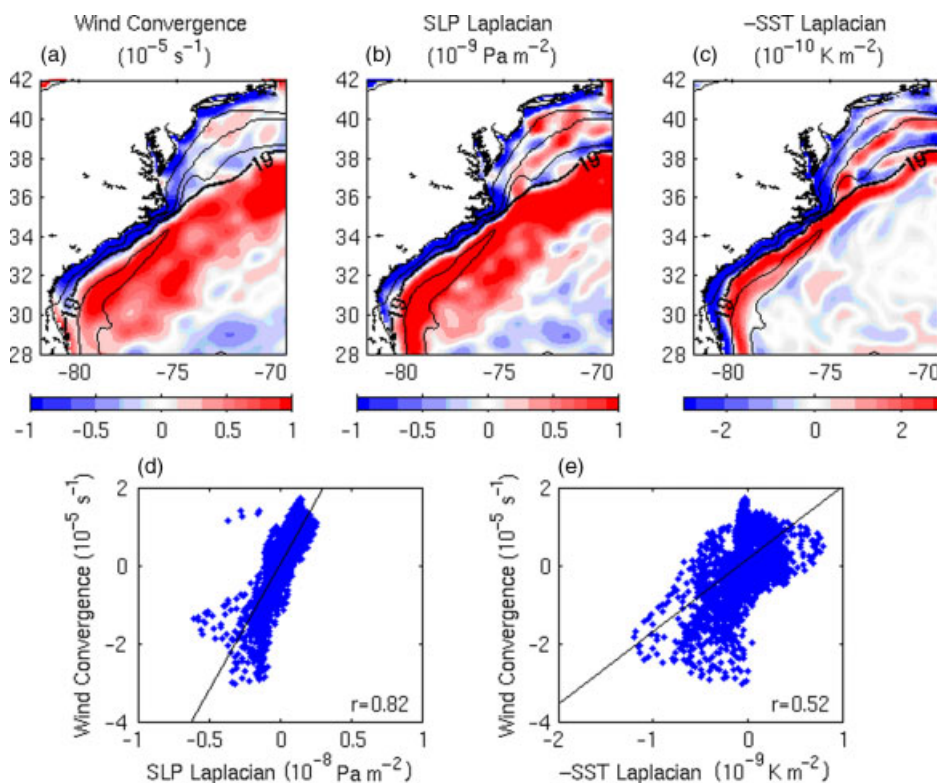
Figure 2. Simulated synoptic mean (averaged over 13–31 January 2005) 10 m wind convergence (a), mean SLP Laplacian (b), and mean SST Laplacian with the sign reversed (c). Contours on (a–c) are for mean SST (4 °C interval). Also presented are the point-to-point comparisons between mean wind convergence and mean SLP Laplacian (d), and between mean wind convergence and −SST Laplacian (d). In both (d) and (e), the linear regression line and its corresponding correlation coefficient are given.

aligned with the 19 °C isotherm (e.g. GS SST front), comparing nicely to the spatial distributions of the annual and seasonal (December–January–February) mean convergence given by Minobe *et al.* (2008, 2010). The convergence maxima are an order of magnitude stronger than the seasonal mean convergence observed by Minobe *et al.*, (2010), and located where the strong northerly winds off the continent first encounter the SST front over the warm GS waters. We also note a smaller local convergence zone over the Middle Atlantic Bight (MAB) shelfbreak where a shelfbreak front is known to exist (Linder and Gawarkiewicz, 1998).

To understand the mechanism that drives synoptic wind convergence along the GS, we examine a simple, linear theoretical model based on geostrophic and Ekman dynamics proposed by Minobe *et al.* (2008):

$$\varepsilon u - fv = -\frac{P_x}{\rho_0} \qquad (1)$$

$$\varepsilon v + fu = -\frac{P_y}{\rho_0} \qquad (2)$$

where u and v are the 10 m across-shelf and along-shelf velocity components, P is sea level pressure, ε is a constant frictional damping coefficient, f is the Coriolis parameter, and ρ_0 is the air density. If we cross-differentiate these equations, we get:

$$\varepsilon u_x - fv_x = -\frac{P_{xx}}{\rho_0} \qquad (3)$$

$$\varepsilon u_y - fv_y = -\frac{P_{xy}}{\rho_0} \qquad (4)$$

$$\varepsilon v_x + fu_x = -\frac{P_{xy}}{\rho_0} \qquad (5)$$

$$\varepsilon v_y + fu_y = -\frac{P_{yy}}{\rho_0} \qquad (6)$$

Adding Equations (3) and (6) and subtracting Equations (4) and (5) to eliminate the pressure terms results in:

$$\varepsilon(u_x + v_y) + f(u_y - v_x) = -\frac{(P_{xx} + P_{yy})}{\rho_0} \qquad (7)$$

$$\varepsilon(u_y - v_x) - f(v_y + u_x) = 0 \qquad (8)$$

Equation 8 can be rearranged to solve for $(u_y - v_x)$ so that $(u_y - v_x) = f/\varepsilon(u_x + v_y)$. A simple substitution of $(u_y - v_x)$ into Equation 7 gives:

$$\varepsilon(u_x + v_y) + \frac{f^2}{\varepsilon(u_x + v_y)} = -\frac{(P_{xx} + P_{yy})}{\rho_0} \qquad (9)$$

Finally, by combining the convergence terms and reorganizing the remaining terms we obtain:

$$-(u_x + v_y)\rho_0 = \frac{(P_{xx} + P_{yy})\varepsilon}{(\varepsilon^2 + f^2)} \qquad (10)$$

which as Minobe *et al.* (2008) indicates, shows that surface wind convergence is proportional to the Laplacian of SLP.

Lindzen and Nigam (1987) uses a simplified mathematical model to examine locally forced MABL convergence and resulting rainfall patterns over tropical oceans. In their model, SST gradients induce SLP gradients based on the following first-order relationship: $P = g\rho_0 nH_0(\gamma/2 - 1)T$, where T is the SST, P is the SLP, γ is a constant, g is gravitational acceleration, H_0 is the equivalent depth of the atmosphere, and n is the local derivative of air density over temperature $-(1/\rho)(\partial\rho/\partial T)$. Since this equation indicates that SLP is linearly forced by SST, it can be further deduced that surface wind convergence is also proportional to the Laplacian of SST, i.e. $-(u_x + v_y)\rho_0 \sim -(T_{xx} + T_{yy})$.

Indeed the spatial patterns of the synoptic mean SLP Laplacian (Figure 2(b)) are strikingly similar to the mean surface wind convergence (Figure 2(a)), particularly in the breadth of the convergence zone and the meandering along the 19 °C isotherm associated with the mean position of the GS SST front. Positive SLP Laplacian, indicating pressures that are lower than the surrounding mean pressure, shows excellent correspondence to the surface wind convergence zone. Point-by-point comparisons indicate the mean wind convergence is linearly related to SLP Laplacian with a correlation of 0.82 (Figure 2(d)). Likewise, the relationship between the mean surface wind convergence and mean sign-reversed SST Laplacian (representing where SST has dropped more than the adjacent mean ocean temperature) is pronounced over the coastal areas and along the length of the GS front. Although this correspondence begins to break down further offshore, the linear relationship is still maintained with a positive correlation of 0.52 over the entire study domain (Figure 2(e)). We found through a set of model sensitivity experiments that this correlation in particular was significantly better using the two-way coupled atmosphere–ocean model configuration compared to our sensitivity runs where SST bottom boundary layer condition was held stationary or supplied at very coarse spatial and temporal resolution.

This analysis suggests that the air–sea interactions over the GS during moderate to strong winter storms quickly destabilizes the atmosphere by modifying the overlying atmospheric temperature, pressure, and wind fields. Initially, the ocean loses heat to the atmosphere primarily along the length of the GS front due to persistent cooling associated with the frequent passage of ETCs. Heat fluxes warm the MABL and generate an area of relatively low pressure offshore. Low SLP anomalies cause surface winds to accelerate offshore and converge over the GS.

To further illustrate the dynamic coupling between the ocean and atmosphere during east coast ETC outbreaks, we examine vertical profiles of synoptic mean vertical wind velocities from sea level to 800 mb in relation to −SST Laplacian and SLP Laplacian along
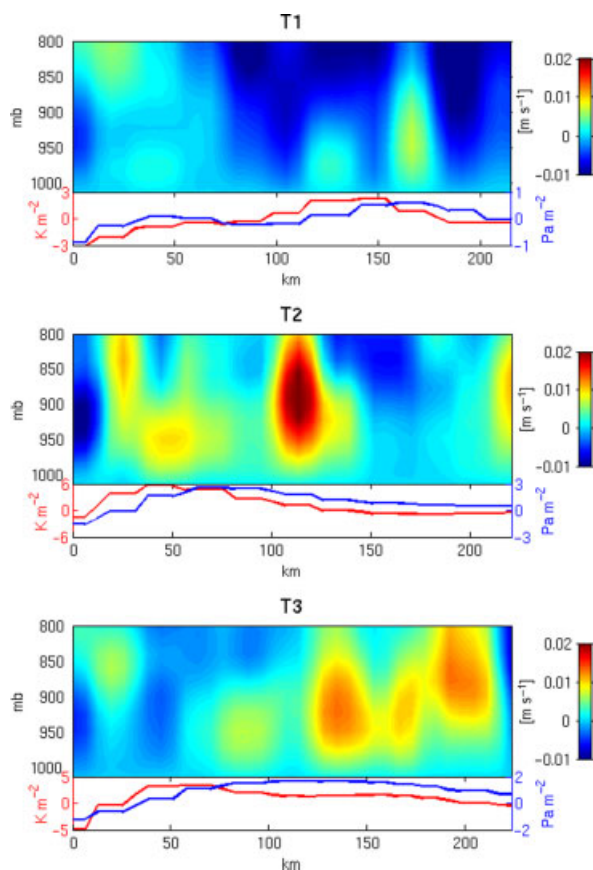
Figure 3. Vertical profiles of simulated synoptic mean wind vertical velocity (shaded; upward positive, m s^{-1}) along three cross-shelf transects (locations of T1, T2, and T3 shown in Figure 1). Also shown at the bottom of each panel are along-transect $-$SST Laplacian (red; 10^{-10} K m^{-2}) and SLP laplacian (blue; 10^{-9} Pa m^{-2}).

three cross-shelf transects (Figure 3). Transects T1-3 span the cool waters of the northern MAB shelf, the GS near Cape Hatteras, and the GS in the South Atlantic Bight (SAB), respectively (see their locations in the inset panel of Figure 1). Lateral distributions of vertical motions in the MABL correspond well with the along-transect Laplacian of SLP and $-$SST. The stronger, more-defined upward motions, indicated by large positive vertical velocity, occur slightly seaward of the maximum SLP Laplacian which peaks just seaward of the $-$SST Laplacian. Moderate vertical velocities are co-located with peaks in $-$SST Laplacian, particularly over the GS SST front about 50 to 100 km from the shoreward end of transects T2 and T3. On the basis of the relationship between surface wind convergence and SLP Laplacian, our analysis suggests that the upward vertical motions anchored over the GS (T2 and T3) are triggered by strong surface convergence which is induced by the SST gradient (as in Lindzen and Nigam's (1987) model).

4. Summary and conclusion

We utilize a high-resolution, regional scale air$-$sea-coupled model (WRF/ROMS configuration of the COAWST modeling system) to simulate five east coast ETCs from 13 to 31 January 2005. Very good agreements are found between buoy-observed and model-simulated surface winds, SLP, air temperature, and SST. Coupled model diagnostics reveal a clearly defined band of maximum surface wind convergence co-located with the warm GS waters. Complementary to Minobe *et al.* (2008, 2010) studies on the GS effect on seasonal and annual mean wind convergence, our study shows that surface wind convergence and the Laplacian of SLP and Laplacian of $-$SST are proportionate even on the synoptic (1$-$2 weeks) time scale. Strong air$-$sea interactions during winter ETC outbreaks, particularly the low SLP anomalies offshore and enhanced ocean heat loss, generate the GS surface wind convergence zone and the subsequent upward motions throughout the MABL, supporting rapid ETC intensification off the eastern US seaboard.

It can be concluded that in order to improve ETC predictions and regional coastal wind and wind energy potential assessment in general, such strong air$-$sea interactions affecting momentum and buoyancy flux exchanges have to be accurately accounted for in an atmosphere$-$ocean coupled modeling framework.

Acknowledgements

References

Bane JM, Osgood KE. 1989. Wintertime air-sea interaction processes across the Gulf Stream. *Journal of Geophysical Research* **94**: 10755$-$10772.

Colucci SJ. 1976. Winter cyclone frequencies over the eastern United States and adjacent western Atlantic, 1964$-$1973. *Bulletin of the American Meteorological Society* **57**(5): 548$-$553.

Dirks RA, Kuettner JP, Moore JA. 1988. Genesis of Atlantic Lows Experiment (GALE): an overview. *Bulletin of the American Meteorological Society* **69**(2): 148$-$160.

Doyle JD, Warner TT. 1990. Mesoscale coastal processes during GALE IOP 2. *Monthly Weather Review* **118**: 283$-$308.

Hirsch ME, DeGaetano AT, Colucci SJ. 2001. An east coast winter storm climatology. *Journal of Climate* **14**: 882$-$899.

Holt T, Raman S. 1990. Marine boundary-layer structure and circulation in the region of offshore redevelopment of a cyclone during GALE. *Monthly Weather Review* **118**: 392$-$410.

Huang C-Y, Raman S. 1988. A numerical modeling study of the marine boundary layer over the Gulf Stream during cold air advection. *Bound-Layer Meteorology* **45**: 251$-$290.

Jones PW. 1998. A user's guide for SCRIP: a Spherical Coordinate Remapping and Interpolation Package, Los Alamos National Laboratory (http://climate.lanl.gov/Software/SCRIP/).

Joyce TM, Kwon Y-O, Yu L. 2009. On the relationship between synoptic wintertime variability and path shifts in the Gulf Stream and the Kuroshio Extension. *Journal of Climate* **22**: 3177$-$3192.

Larson J, Jacob R, Ong E. 2005. The Model Coupling Toolkit: a new FORTRAN90 toolkit for building multiphysics parallel coupled models. *International Journal of High Performance Computing Applications* **19**(3): 277–292.

Li Y, Xue H, Bane JM. 2002. Air-sea interactions during the passage of a winter storm over the Gulf Stream: a three-dimensional coupled atmosphere-ocean model study. *Journal of Geophysical Research* **107**: 1–13.

Linder CA, Gawarkiewicz G. 1998. A climatology of the shelfbreak front in the Middle Atlantic Bight. *Journal of Geophysical Research* **103**: 18405–18423.

Lindzen RS, Nigam S. 1987. On the role of sea surface temperature gradients in forcing low-level winds and convergence in the tropics. *Journal of the Atmospheric Science* **44**(17): 2418–2436.

Minobe S, Kuwano-Yoshida A, Komori N, Xie S-P, Small RJ. 2008. Influence of the Gulf Stream on the troposphere. *Nature* **452**: 206–210, DOI: 10.1038/nature06690.

Minobe S, Miyashita M, Kuwano-Yoshida A, Tokinaga H, Xie S-P. 2010. Atmospheric response to the Gulf Stream: seasonal variations. *Journal of Climate* **23**: 3699–3719, DOI: 10.1175/2010JCLI3359.1.

Raman S, Reddy NC. 1996. Numerical simulation of a mesolow over a Gulf Stream Filament. *Pure and Applied Geophysics* **147**: 789–819.

Sanders F, Gyakum JR. 1980. Synoptic-dynamic climatology of the "bomb". *Monthly Weather Review* **108**: 1589–1606.

Shchepetkin AF, McWilliams JC. 2005. The regional oceanic modeling system (ROMS): a split-explicit, free-surface, topography-following-coordinate oceanic model. *Ocean Modelling* **9**: 347–404.

Skamarock WC, Klemp JB, Dudhia J, Gill DO, Barker DM, Duda MG, Huang X-Y, Wang W, Powers JG. 2008. *A description of the Advanced Research WRF Version 3, NCAR Technical Note*. Mesoscale and Microscale Meteorology Division, National Center for Atmospheric Research: Boulder, CO.

Small RJ, deSzoeke SP, Xie SP, O'Neill L, Seo H, Song Q, Cornillon P, Spall M, Minobe S. 2008. Air-sea interactions over ocean fronts and eddies. *Dynamics of Atmospheres and Oceans* **45**: 274–319.

Song Q, Cornillon P, Hara T. 2006. Surface wind response to oceanic fronts. *Journal of Geophysical Research* **111**: C12006.

Warner JC, Armstrong B, He R, Zambon JB. 2010. Development of a Coupled-Ocean-Atmosphere-Wave-Sediment Transport (COAWST) modeling system. *Ocean Modelling* **35**(3): 230–244, DOI: 10.1016/j.ocemod.2010.07.010.

Xue H, Pan Z, Bane JM. 2000. A 2D coupled atmosphere-ocean model study of air-sea interactions during a cold air outbreak over the Gulf Stream. *Monthly Weather Review* **128**: 973–996.

Zishka KM, Smith PJ. 1980. The climatology of cyclones and anticyclones over North America and surrounding ocean environs for January and July, 1950–77. *Monthly Weather Review* **108**(4): 387–401.